CAAP Quarterly Report

Date of Report: April 10, 2015

Contract Number: DTPH56-14-S-N000006 DTPH5614HCAP07

Prepared for: Government Agency: DOT

Project Title: Laser peening for preventing pipe corrosion and failure

Prepared by: Board of Regent of the University of Nebraska for the University of Nebraska–Lincoln

Contact Information: Yongfeng Lu
Lott Distinguished Professor
Department of Electrical and Computer Engineering, University of Nebraska- Lincoln, 209N Walter Scott Engineering Center, Lincoln, NE 68588-0511
Phone: (402) 472-8323
E-mail: ylu2@unl.edu

For quarterly period ending: March 31, 2015

Business and Activity Section

(a) Status Update of Past Quarter Activities

1. The major goal of the project

The ultimate goal of this project is to investigate and develop laser peening of pipeline steels to improve the corrosion resistance of stainless steel and carbon steel used for pipeline construction. The corrosion resistance of pipelines will be enhanced *via* the compressive residual stress created by laser-induced shock waves during laser peening. It is anticipated that by using laser shock peening in the construction of a pipeline, the reliability, safety, and lifespan of the nation's pipeline transportation system will be highly improved. As stated in our proposal, the major goals of this project include four phases with associated objectives. Table 1 summaries the current progress for the objectives in each phase as of this reporting period.

Table 1. The completion rate for each phase objective of the project.

Phases	Major goals and milestones	Starting date (mm/dd/yy)	Ending date (mm/dd/yy)	Completion rate (%)
Phase 1	1) Experimental setup for laser cleaning developed	10/01/2014	12/31/2014	100
	2) Cleaning mechanism and parameter windows	01/01/2015	09/30/2016	0
	3) Real-time monitoring of cleaning process	01/01/2015	09/30/2016	0
Phase 2	1) A laser peening system developed	10/01/2014	12/31/2014	100
	2) Parameter windows for laser peening established	01/01/2015	09/30/2016	50
Phase 3	1) Surface morphology study of the laser-peened surfaces	01/01/2015	09/30/2016	50
	2) The residual stress of pipeline steels after laser cleaning and peening	01/01/2015	09/30/2016	30
	3) The corrosion resistance of laser-peened surface	01/01/2015	09/30/2016	0
Phase 4	Design a laser peening prototype system	06/30/2016	09/30/2016	0

The specific objectives during this reporting period

During this reporting period of the project (January 1, 2015, to March 31, 2015), the experimental setup for laser shock peening (LSP) has been improved. The processing parameters (including laser energy, spot size, wavelength, and sacrificial coating, etc.) for LSP have been further optimized. The effects of LSP on the surface topography, nano-/microhardness, elastic modulus, and surface compressive residual stresses of the samples manufactured. The samples, Al-Mg alloy, stainless steel and carbon steel, were experimentally investigated and analyzed. The phased objectives and specific content are listed as follows:

(1) Improvement of the experimental setup for laser shock peening.
(2) Preparation of the tested materials (Al-Mg alloy, stainless steel, and carbon steel) for laser shock peening.
(3) Optimization of the processing parameters (laser energy, spot size, wavelength, and sacrificial coating) for laser shock peening.
(4) Metal surface morphology control by LSP.
(5) Study of the surface nano-/microhardness and elastic modulus of the laser-peened samples.
(6) Study of the surface compressive residual stresses of the laser-peened samples using X-ray diffraction $\sin^2\psi$ method.

2. Significant results

2.1 Experimental

2.1.1 Principle and experimental procedure of LSP

LSP is a cold mechanical process where pressure waves caused by expanding plasma plastically deform the surface of a material. LSP uses a thin layer of ablative material that is opaque to the laser. The opaque ablative material, typically black spray paint or tape, is used as a sacrificial layer in an early study by Fairland and Clauer [1]. The sacrificial layer also minimizes thermal effects on the surface caused by the laser. The laser partially vaporizes the ablative layer to form high pressure plasma. The plasma, confined by a thin layer of water film (confining medium), expands rapidly resulting in a recoiling pressure wave on the order of GPa reported by Fariland et al. and Caslaru, et al. [2-3]. The pressure wave is a cold mechanical process that typically deforms the surface. The plasma-induced shock pressure causes severe plastic deformation, refined grain size, compressive residual stresses, and increased hardness at the surface and in the subsurface. As a result, the mechanical properties on the work piece surface are enhanced and the performance of preventing corrosion and foreign objective damage is improved.

2.1.2 Material preparation

During this reporting period, the samples tested were prepared from 304 stainless steel (SS), carbon steel (CS), and Al-Mg alloy plates. The samples of 304 SS, CS, and Al-Mg alloy tested were cut into rectangular shapes with dimensions of 25×25×2 mm^3 (width × length × thickness), 10×10×2 mm^3, and 30×30×2 mm^3, respectively. Information on the chemical compositions and mechanical properties of 304 SS, and Al-Mg alloy were given in the last quarterly report.

Figure 1 shows the (a) scanning electron microscopy (SEM) image of CS and energy dispersive X-ray (EDX) mapping of the main elements in the area indicated by the box in (a). The chemical composition and mechanical properties of CS are shown in Tables 2 and 3, respectively. Prior to the LSP treatment, the samples were polished mechanically with sandpaper of different grades of roughness to achieve a mirror-like surface, which enabled the microhardness and nanoindentation tests requiring a low surface roughness of several hundred nanometers. After careful polishing, the average surface roughness of 304SS, CS, and Al-Mg alloy was reduced to 12, 48, and 55 nm, respectively, as is shown in Fig. 2. The polishing was followed by ultrasonic cleaning, first with acetone/methanol and then deionized water, to degrease the sample surface.

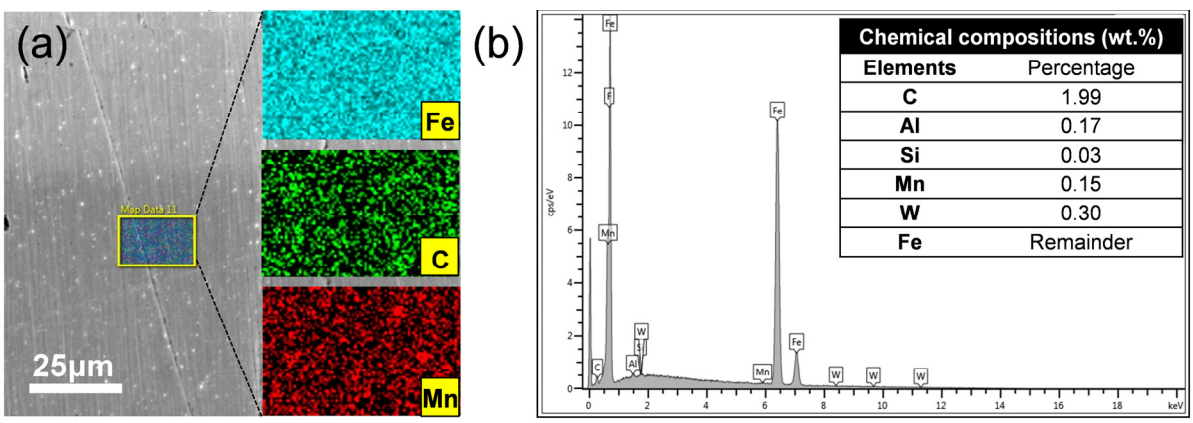

All samples were prepared shortly before the LSP experiments.

Fig. 1. (a) SEM image of carbon steel sample. Inset in (a) shows EDX mappings of Fe, C, and Mn elements in the area indicated by the box in (a); (b) corresponding EDX spectrum and percentage weight of chemical compositions.

Table 2. Chemical compositions of the carbon steel (wt.%) tested.

Composition	C	Al	Si	Mn	W	S	Fe
Percent (wt. %)	1.99	0.17	0.03	0.15	0.30	0.13	Remainder

Table 3. Mechanical properties of the carbon steel tested				
Type	Yield strength (kgf mm^{-2})	Tensile strength (kgf mm^{-2})	Elongation (%)	Specific gravity (g cm^{-3})
Value	290	655	55 (50.8mm)	7.93

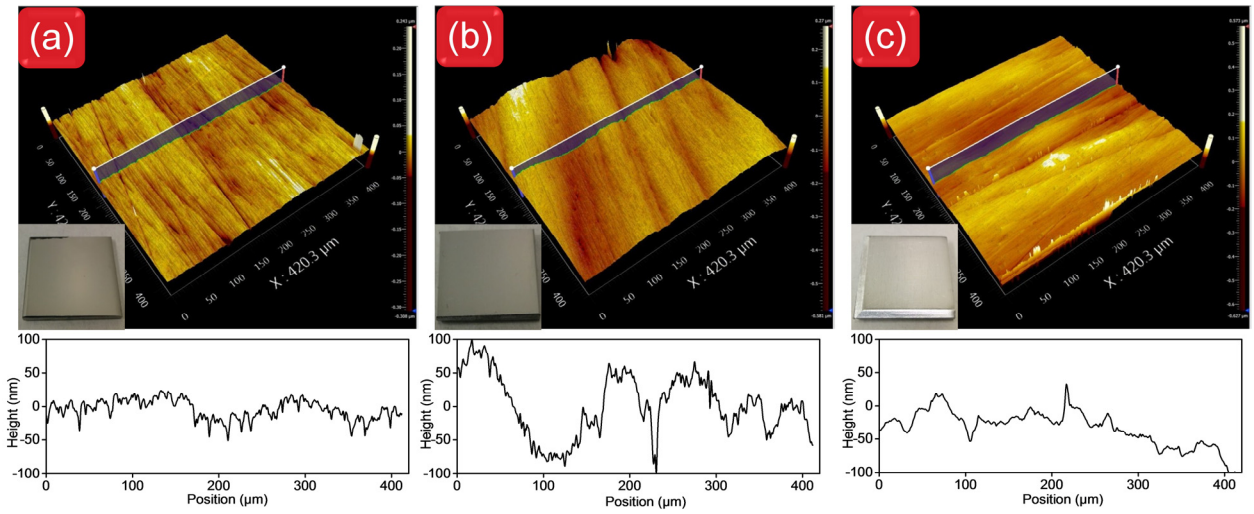

Fig. 2. Three dimensional (3D) surface topographies of the (a) 304 SS, (b) CS, and (c) Al-Mg alloy surfaces by polishing treatment. Insets in (a-c) show the corresponding optical images of the samples in the same images.

2.1.3 Improved experimental setup

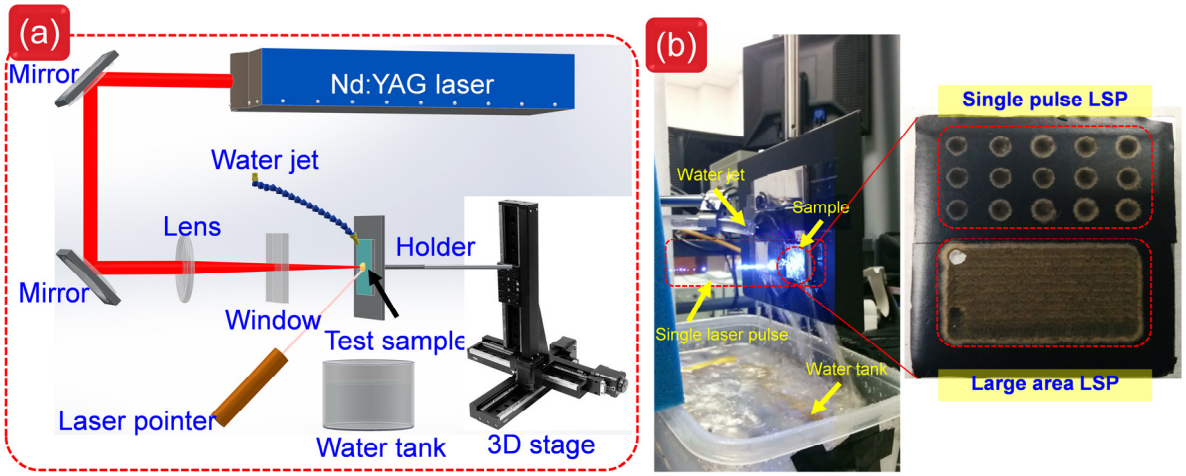

Fig. 3. (a) Schematic of the improved LSP system established in LANE lab, (b) real-time LSP process.

As shown in Fig. 3(a-b), the experimental setup for the LSP system generally remained unchanged except for improvements in two main aspects: 1) the 3D stage used to hold the sample was changed from a six-axis work stage to a three-axis work stage with faster moving

speed and a larger moving range in order to eliminate the mechanical hysteresis error induced by the six-axis work stage, and 2) a new pump-based water cycle system was implemented in the LSP system to replace the previous running water assembly to form a more stable, thin water layer on the sample surface, which helped to improve control accuracy of the water layer thickness.

The main LSP process parameters are listed in Table 4. The laser source was a continuum Q-switched Nd:YAG PR II 8010 laser. During this quarter, different laser pulse energies at 1064 nm wavelength (from 100 to 850 mJ) and at 532 nm (from 50 to 280 mJ) were used. Black tape with a thickness of 177 μm was used as the sacrificial layer. In order to avoid the influence of the water spray induced by laser ablation during laser-material interaction, the focusing lens was changed from a 20 cm focal length to a 50 cm focal length. Two different LSP experiments were designed: a single spot LSP experiment and a large area LSP experiment, from which two kinds of laser-peened samples were obtained (Fig. 3b). The single spot laser-peened samples can be used for depth, morphology, nanoindentation, and microhardness tests, while large area laser-peened samples can be used for compressive residual stress measurement.

Table 4. The processing parameters used in the LSP experiment.

Type	Values
Laser type	Continuum Nd:YAG PR II 8010 laser
Laser pulse energy (mJ)	100 ~ 850 (1064nm); 50~280 (532nm)
Pulse duration (nm)	6 ~ 8
Frequency (Hz)	1 ~ 10
Wavelength (nm)	532, 1064
Laser beam size (mm)	~ 1
Sacrificial coating	Black tape (177 μm)
Confining medium	Flowing water (1 ~ 2 mm)

2.1.4 Characterization

After LSP, the surface quality of the processed samples was systemically investigated to evaluate the LSP effects and optimize the LSP parameters. Optical microscopy (Nikon ECLIPSE, Japan) and electrical scanning microscopy (SEM, Philips, XL 30E, 5kV) were used to study the morphology of laser-peened samples. A 3D profiler (New View 8000, Zygo Corporation) was used to measure the 3D profiles of the macro plastic deformation from the bottom surface of the samples. The micromechanical properties of all samples tested were carried out using a Hysitron nanoindenter with the standard three-sided pyramidal Berkovich (TI-00039) probe and Tukon 2500 Vickers & Knoop microhardness tester with the square-based diamond pyramid indenter. Surface residual stress measurements were conducted by two kinds of X-ray diffraction (XRD) equipment. One is a Rigaku Smartlab with Cu as the anode target, used for Al alloy tests, and the

other is a Rigaku D Max B with Cr as the anode target, which was adopted for 304 SS and CS tests.

2.2 Results and discussion

2.2.1 Further optimization of the processing parameters of LSP using Al-Mg alloy

The important processing parameters related to LSP conditions were the laser processing parameter, confining medium, and sacrificial coatings, which can significantly affect the mechanical properties of the alloy and metallic materials. In the last quarterly report, we had mainly investigated the effects of the sacrificial coatings and the confining medium on the LSP, where the black tape and flowing water were optimized to be the sacrificial material and the suitable confining medium, respectively. The objective of this quarter was to investigate the effect of laser processing parameters (including laser energy, spot size, and wavelength) on LSP in metal components using Al-Mg alloy as the tested samples. The use of Al-Mg alloy was due to its low hardness, which could display more obvious LSP phenomena and thus was much easier for analysis.

(A) Laser pulse energy and spot size effects

Figure 4 shows the relationship between laser pulse energy/fluence density and the spot size under two different wavelengths of 1064 nm (4a-b) and 532 nm (4c-d). At a wavelength of 1064 nm, the laser spot diameter increased exponentially from 0.6 to 1.3 mm with laser pulse energy increasing from 100 to 900 mJ (Fig. 4a), from which a peak laser fluence density of approximately 102 J/cm^2 was obtained at a moderate laser output energy of 650 mJ and corresponding spot diameter of 0.9 mm (Fig. 4b). On the other hand, at a wavelength of 532 nm, a linear relationship between spot diameter and laser pulse energy was observed, as shown in Fig. 4c, leading to peak power density of approximately 48 J/cm^2 at nearly the highest pulse energy and spot size (Fig. 4d). The relationship between spot diameter and laser energy for wavelengths of 1064 nm and 532 nm was different, which should be attributed to limited pulse energy at 532 nm (less than 300 mJ). In fact, for a pulse energy of less than 650 mJ (with peak fluence density) at 1064 nm, the spot size also increased linearly with laser energy.

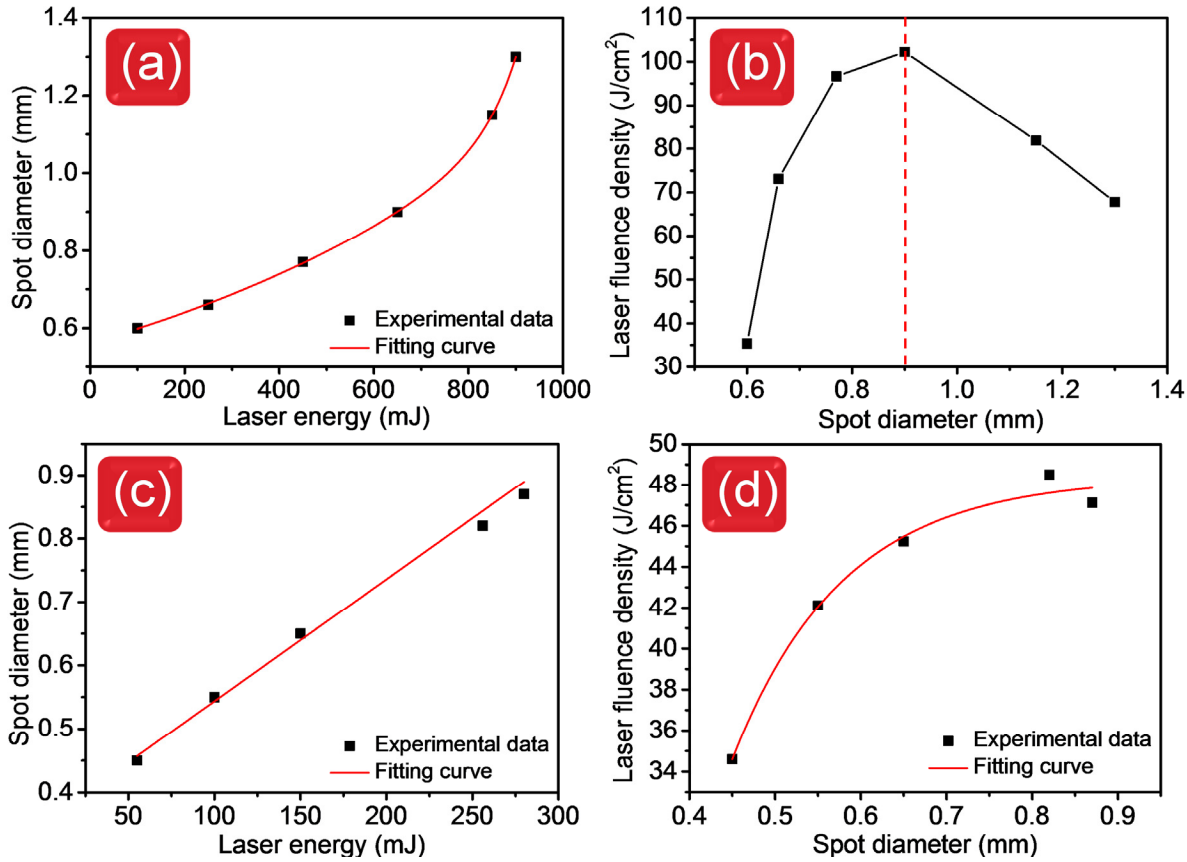

Fig. 4. Dependence of (a) spot diameter on laser energy and (b) laser fluence on spot diameter with 1064 nm wavelength; dependence of (c) spot diameter on laser energy and (d) laser fluence on spot diameter with 532 nm wavelength.

After confirming the relationship between laser pulse energy and spot size, different laser pulse energies from 100 to 850 mJ were used for laser shock peening on Al-Mg alloy surfaces. Figure 5 compares the 3D morphologies (a-e) and optical images (f-j) of the Al-Mg alloy surfaces treated by single-pulse LSP with a laser energy of (a, f) 100, (b, g) 250 (c, h) 450, (d, i) 650, and (e, j) 850 mJ. The cross-section profile of the dent along the lines in Fig. 5 (a-e) is shown in Fig. 5k, demonstrating the obvious increase in both dent depth and dent diameter with the increment of laser pulse energy. Specifically, the dent diameter as a function of laser pulse energy is shown in Fig. 5I. The dent diameter was increased rapidly with the increment of laser energy, which was similar to the relationship between spot diameter and laser pulse energy (Fig. 4a).

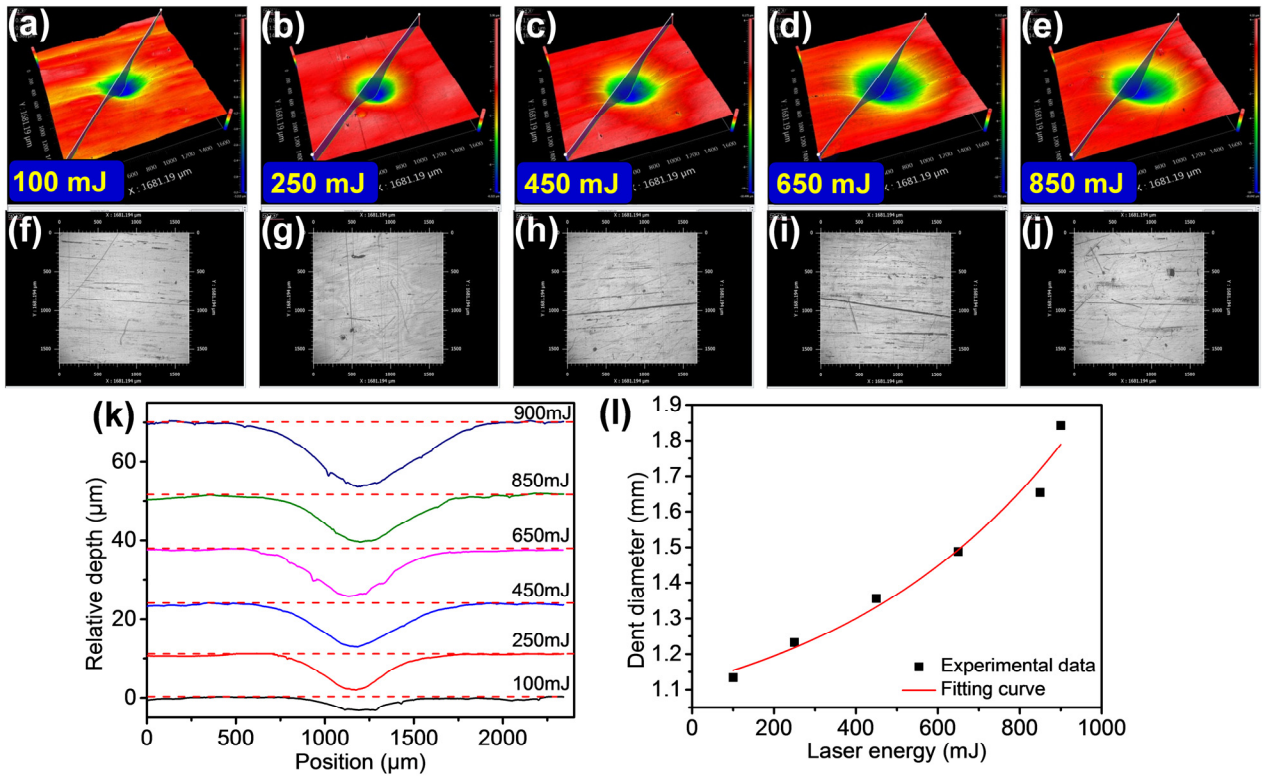

Fig. 5. (a-e) 3D surface topographies of the Al-Mg alloy surfaces treated by single pulse LSP with laser energy of (a) 100, (b) 250, (c) 450, (d) 650, and (e) 850 mJ. (f-i) Corresponding optical images of the Al-Mg alloy shown in (a-e). (k) Dent depths with different laser energy. (l) The dent diameter as a function of laser energy.

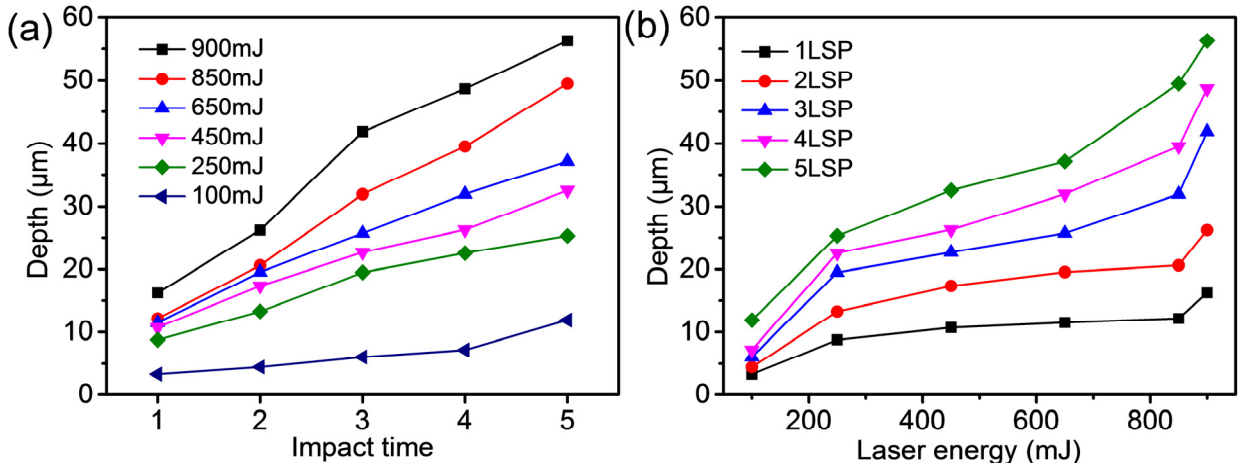

Fig. 6. The depth of the dent center as a function of (a) impact time and (b) laser energy.

Figure 6 shows the center depth of the dent on the Al alloy surface as a function of (a) impact time and (b) laser energy. It can be seen from Fig.6a that all the curves for different laser pulse energies are nearly linear but with different slopes. The higher the pulse energy, the bigger the slope, indicating a more effective LSP effect with higher laser energy. Figure 6b plots the dent

depth versus laser pulse energy. Two critical pulse energies can be pointed out. First, at 100 mJ pulse energy, the dent depth increased very slowly; and only with an LSP with five impacts could the dent depth be larger than 10 μm, indicating a serious loss in shock wave pressure and the approach to the limited energy of plasma and shock wave generation. Second, a steep increase was observed from 850 to 900 mJ, which may need further research by laser-induced breakdown spectroscopy (LIBS) and pressure measurement. Overall, the depth at the dent center increased with the incremental increase in both LSP impact times and laser pulse energy. It should be pointed out that although the laser power density decreased from 102 to 68 J/cm^2 and the pulse energy increased from 650 to 900 mJ (Fig. 4b), the dent depth continued to increase at all impact times (Fig. 6b), indicating that both the laser fluence and the spot size contributed to the pressure value of the laser-induced shock wave.

(B) Laser wavelength effect

Laser wavelength is another processing parameter which could affect the shock wave pressure. Therefore, a preliminary experiment was conducted with two different wavelengths of the Nd:YAG laser. The dent depth versus laser pulse energy are plotted under different wavelengths (1064 nm, 532 nm) for one impact and five impacts, respectively, in Fig. 7 (a-b). Compared with the shorter wavelength (532 nm), a longer wavelength (1064 nm) was found to be slightly more efficient for the LSP effect. It is believed that the laser wavelength affects the shock wave in three aspects: 1) absorption coefficient of the water overlay; 2) laser and metal interaction efficiency; and 3) dielectric breakdown threshold of the transmitting medium [4]. In our experiment, although 532 nm had a lower absorption coefficient in water and a higher photon-metal interaction rate compared to 1064 nm, its low dielectric breakdown threshold could result in much more energy cost in laser transmission, thus limiting the shock wave pressure to a value lower than the shock wave generated by the 1064 nm laser pulse with the same energy.

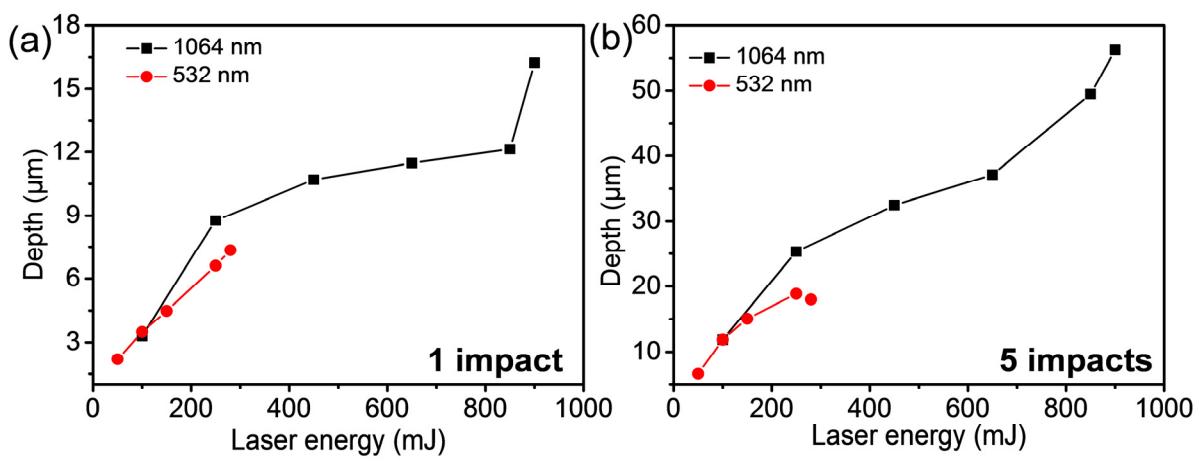

Fig. 7. The depth of the dent center vs. laser energy with laser wavelengths of 1064 and 532 nm for (a) 1, and (b) 5 impacts.

2.2.2 Metal surface morphology control by LSP

(A) The effect of black tape modification on the surface roughness and surface profile

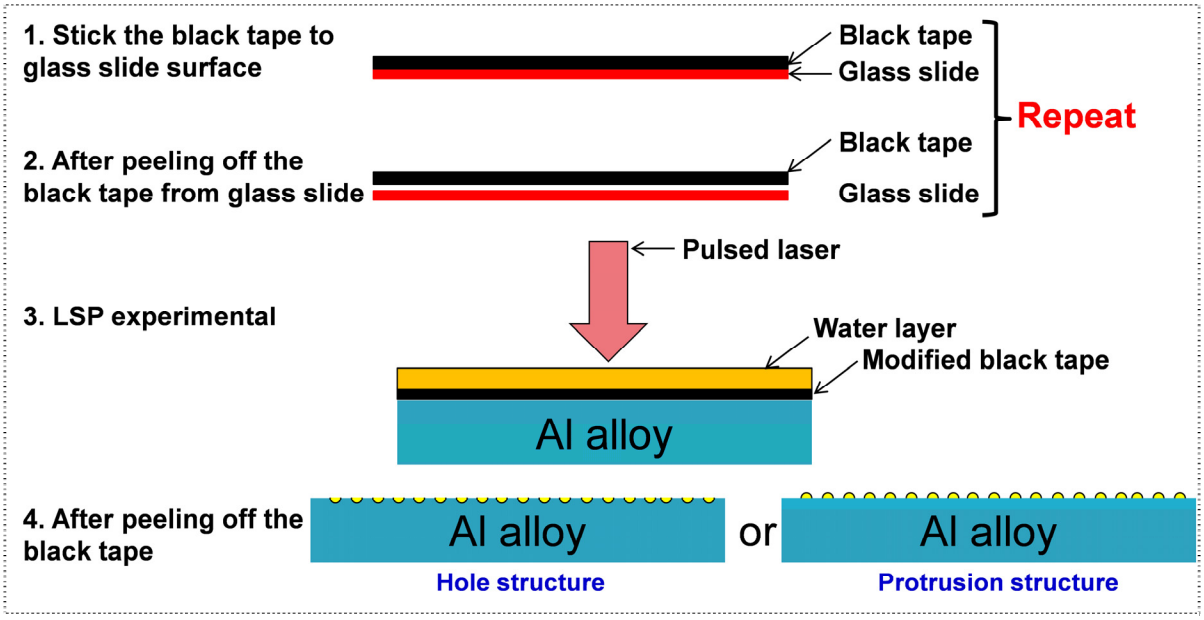

Fig. 8. Schematics of the laser shock-induced hole/protrusion formation process.

During the last quarter, it was recognized that the black tape conditions could result in different structures on the sample surface, such as holes or protrusions. Thus, a procedure in Fig. 8 was designed to quantitatively model different black tape conditions. By sticking the black tape to a glass slide surface and then peeling it off, the change in the black tape surface was achieved. Next, the same treatment was repeated for different times; and the modified black tape was attached to the Al-Mg alloy surface to finish the sample preparation with different black tape conditions. After the LSP experiments, the sample surface structures were examined by a Zygo 3D profile meter and optical images.

For reference, black tape without any treatment was used for the LSP treatment with different impact times. Figure 9 shows the (a-e) 3D surface morphology and (f-j) optical images of the Al-Mg alloy after single spot LSP for one to five impacts. No obvious localized surface roughness was observed, and few microholes/protrudes were found. Similar results were also observed on the surfaces of 304 SS and carbon steel (not shown here). The dent depth as a function of LSP impact times is plotted for Al-Mg alloy (Fig. 9k), 304 SS (Fig. 9l), and carbon steel (Fig. 9m), where the dent depth changed from 20 to 80 μm for Al-Mg alloy, 4 to 11 μm for 304 SS, and 2 to 8 μm for carbon steel. A linear relationship between the dent depth and LSP impact times was observed for different materials but the slopes varied: Al-Mg alloy > 304 SS > carbon steel.

Fig. 10 shows 3D surface topographies and optical images of the Al-Mg alloy surfaces treated by single pulse LSP with black tape sticking to/peeling off from glass slides for (a, e) 0, (b, f) 1, (c,

g) 2, and (d, h) 5 times. Uniform micro holes/protrusions were formed by LSP with modified black tapes. It was observed that by increasing the modification times, the micro holes/protrusions became more intensively distributed; and the hole/protrusion sizes became larger.

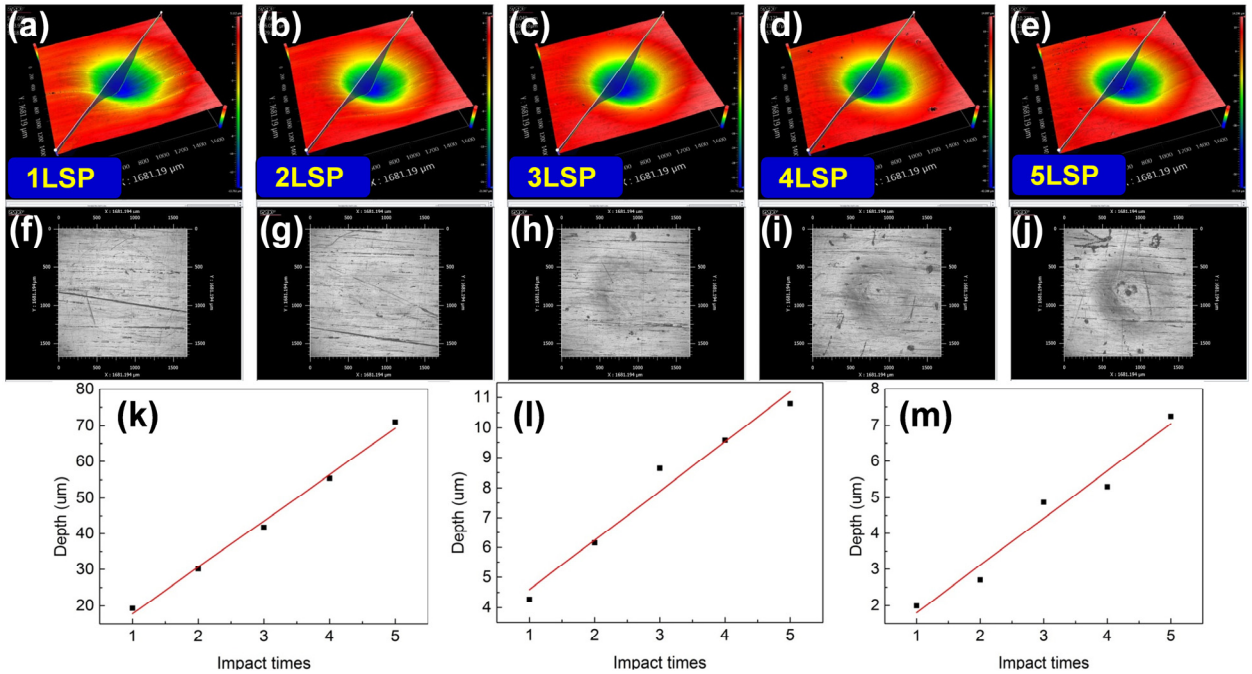

Fig. 9. (a-e) 3D surface topographies of the Al-Mg alloy surfaces treated by single pulse LSP for (a) 1, (b) 2, (c) 3, (d) 4, and (e) 5 impacts. (f-j) Corresponding optical images of the Al-Mg alloy shown in (a-e). Dependence of dent depth on pulsed laser impact time for (k) Al-Mg alloy, (l) 304 SS, and (m) CS.

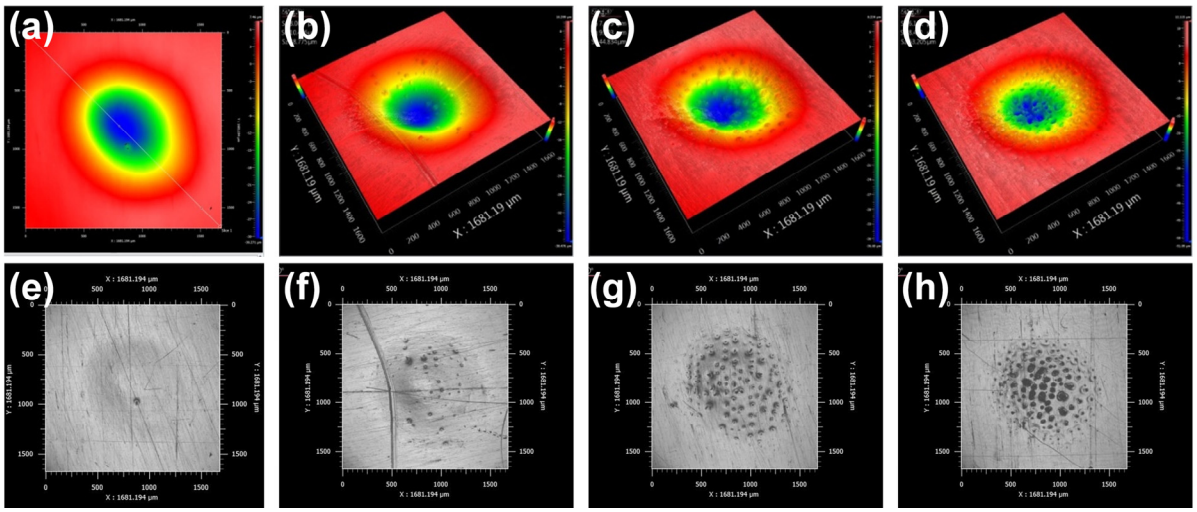

Fig. 10. (a-d) 3D surface topographies of the Al-Mg alloy surfaces treated by single pulse LSP with black tape sticking to/peeling off from glass slide for (a) 0, (b) 1, (c) 2, and (d) 5 times. (e-h) Corresponding optical images of the Al-Mg alloy shown in (a-d).

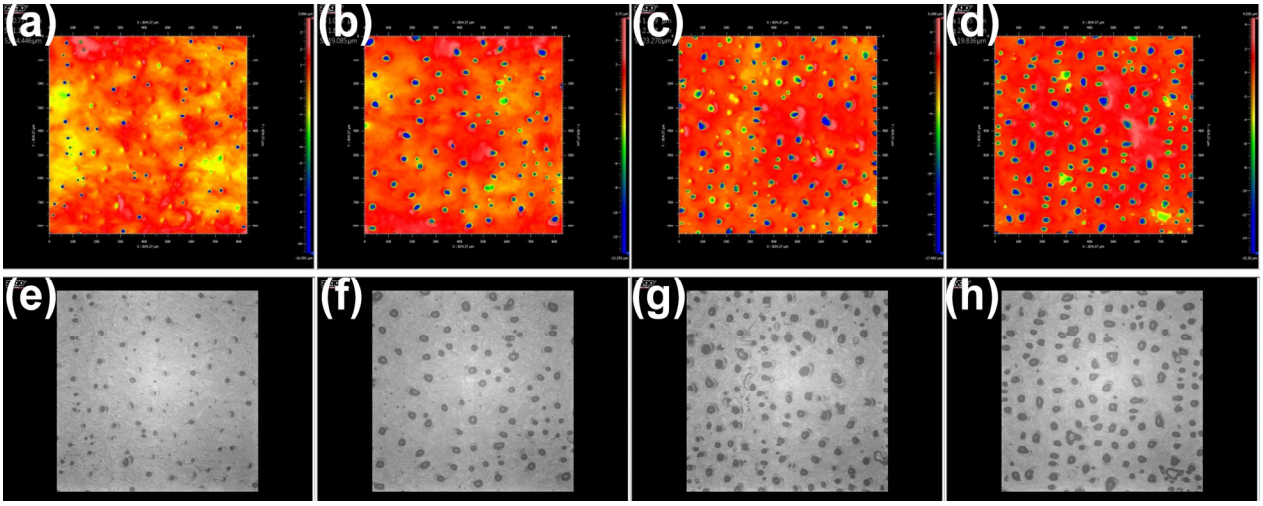

Fig. 11. (a-d) 3D surface topographies of the black tape surfaces (a) without treatment, (b) after sticking to/peeling off from the glass slide (b) 1, (c) 2, and (d) 5 times. (e-h) Corresponding optical images of the black tape shown in (a-d).

In Fig. 11, the surface morphology and optical images of the black tape surface without treatment (Fig. 11 (a,e), with treatment for 1 time (b,f), 2 times (c,g), and 5 times (d,h) indicate that the small holes on the tape surface obviously increased from ~25 μm (0 time) to ~35 μm (1 time), ~40 μm (2 times), and ~50 μm (5 times). The small holes on the black tape surface changed from small and sparse to large and dense as the increasing of the treatment times. It is assumed that the micro holes/protrusions formed on the Al-Mg alloy sample surface were induced by the holes on the surface of the black tape. There should be a threshold for the hole diameter on the black tape surface for the micro dent/protrusion generation on the sample surface.

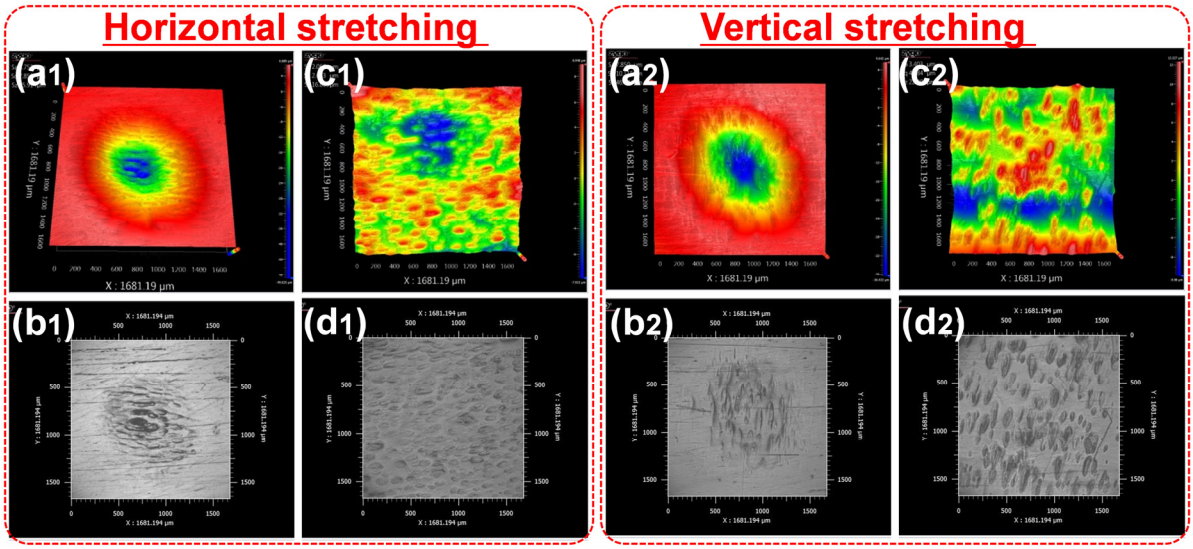

Fig. 12. (a_1-d_1) 3D surface topographies of the Al-Mg alloy surfaces treated by (a_1, b_1) single pulse and (c_1, d_1) large area LSP after black tape horizontal stretching treatment. (a_2-d_2) 3D surface topographies of the Al-Mg alloy surfaces treated by (a_2, b_2) single pulse and (c_2, d_2) large area LSP after black tape vertical stretching treatment.

To confirm the relationship between the tape surface structure and the micro holes/protrusions generated on the sample surface, another tape surface modification method was applied. The black tape was stretched horizontally/vertically and attached to the Al-Mg alloy surface without release. As shown in Fig. 12, with horizontally stretched black tape as the sacrificial layer, the sample surface after both single spot LSP and large area LSP shows long and narrow micro holes/protrusions along the horizontal direction. For single spot LSP, protrusions distributed around and inside the dent except for the center of it (Fig. $12a_1$, b_1). For large area LSP, protrusions distributed extensively and holes are scarce (Fig. $12c_1$, d_1). With vertically stretched black tape attached to the Al-Mg alloy without release, long and narrow holes/protrusions along the vertical direction were observed. The same distribution phenomena of holes/protrusions in a single-spot LSP and large-area LSP applied as the samples with horizontally stretched black tape, except for the direction (Fig. $12a_2$-d_2).

Figure 13 shows the surface morphologies and optical images of black tape without processing (a,f) after stretching horizontally for 120% (b,f), 140% (c,h), and a combination of sticking to/peeling off from a glass slide for five times and horizontally stretching for 120% (d,i) and 140% (e,j). No obvious change in hole diameter was observed by stretching only, while the elongation could easily be observed by combining sticking/peeling and stretching. The 140% stretching led to larger elongation than that by 120% stretching. The spindle holes/protrusion microstructures formed on the laser-peened metal surfaces are believed to have a direct relationship with the small hole elongation on the black tape surface.

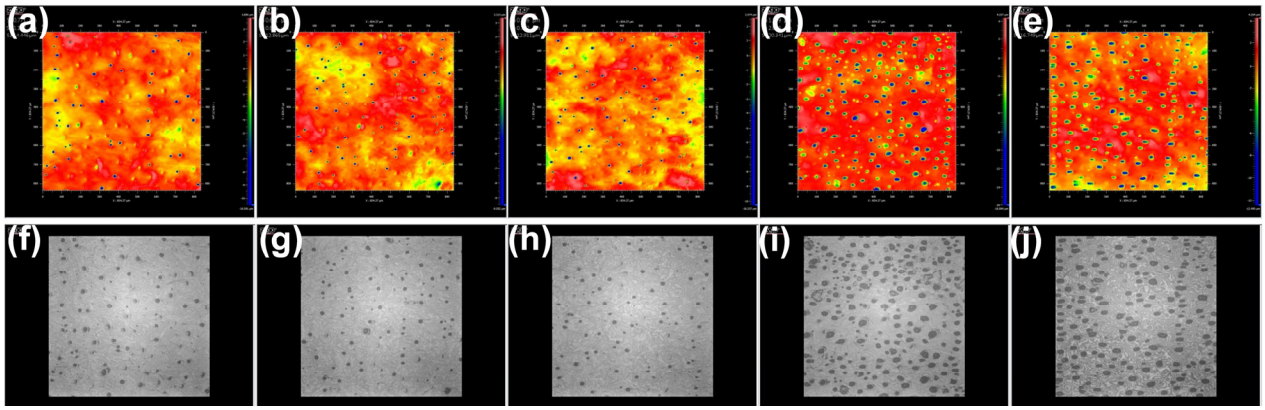

Fig. 13. (a-e) 3D surface topographies of the black tape surfaces (a) without treatment, after stretching with stretch ratio of (b) 120% and (c) 140% and after sticking to/peeling off from glass slide 5 times and then stretching with a stretch ratio of (d) 120% and (e) 140%. (f-j) Corresponding optical images of the black tape shown in (a-e).

In general, the size, shape, and density of the micro holes/protrusion microstructures could be effectively controlled by surface treatment of the black tape before LSP. A close relationship exists between the hole size/structure on the black tape applied and the micro holes/protrusions microstructures generated on the sample surfaces. It is known that the defects on the metal

surface might become the initiation points of corrosion. The research results obtained in this part will help to avoid undesired micro dent/protrusion defects forming on the laser-peened metal surface by carefully controlling the tape and sample preparation process.

(B) The laser shock bending by large area LSP

Laser shock bending is of significant value to the aerospace, automotive, ship building, and microelectronics industries. Conventionally, the laser bending process is achieved by introducing thermal stress into the work piece by irradiation with a focused laser beam. Recently, nonthermal bending using a high energy pulsed laser has generated growing interest. Similar to the laser shock peening process, high-pressure and compressive shock waves are induced onto the target material by high-energy laser pulses. This nonthermal, shock-wave-bending mechanism is often denoted as laser shock bending.

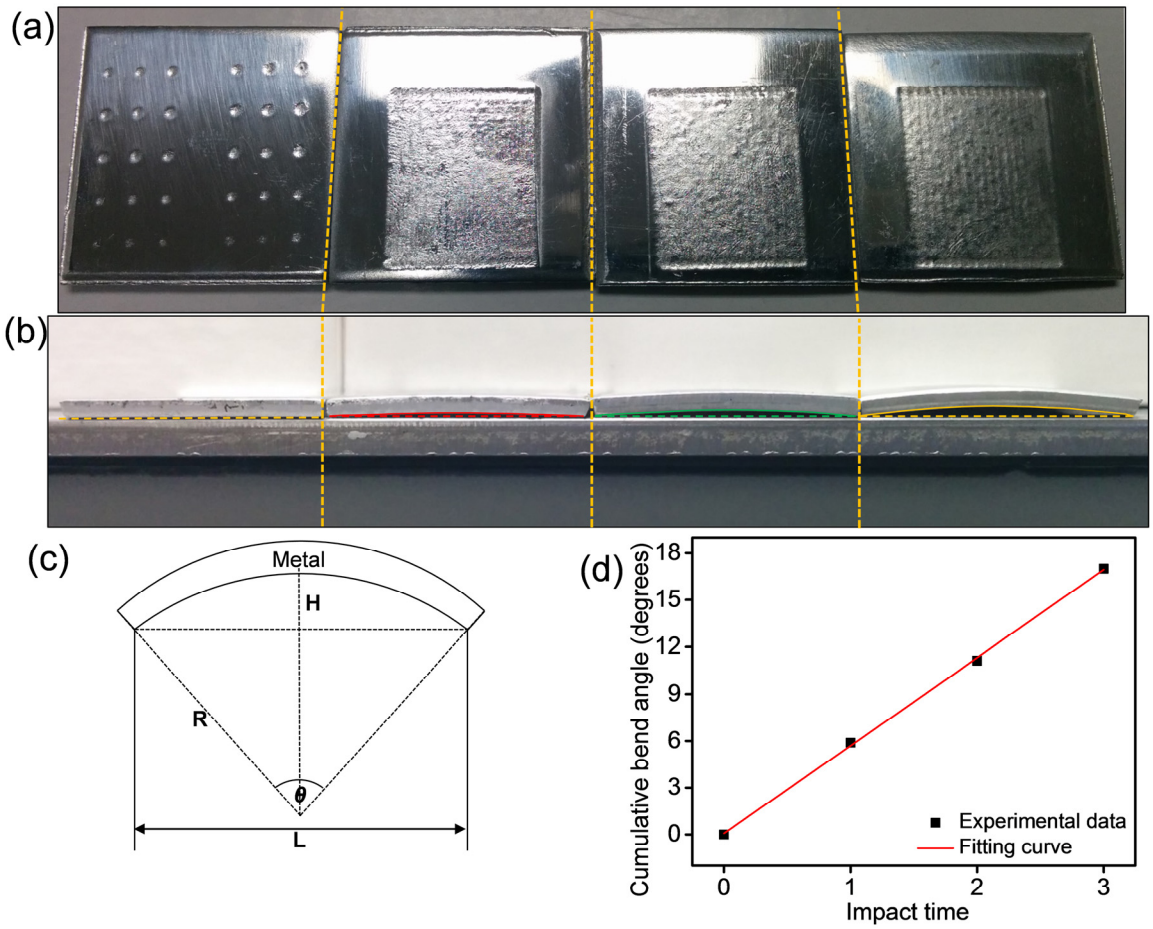

Fig. 14. A large area laser shock peening formed Al-Mg alloy with different impact times. (a) Top view, (b) side view, (c) the model for calculating the laser shock bend angle, (d) dependence of the bend angle of Al-Mg alloy on pulsed laser impact times.

In our lab, the laser shock bending phenomenon has been observed during the large area LSP processing of Al-Mg alloy plates with a thickness of approximately 2 mm, as is shown in Fig. 14.

The sample bending direction is perpendicular to the laser scanning direction. It is clear that the deformation mechanism of this Al-Mg alloy is positive under a laser energy of 800 mJ. The bending angle (Fig. 14(d)) increases linearly with the LSP impact times, changing from 0° before LSP, to 6°, 11°, and 16° after 1, 2, and 3 times the large area LSP, respectively. It is considered that the deeper compressive stress achieved by LSP leads to the formation of tighter curvatures.

2.2.3 Surface hardening induced by LSP

Surface hardness measurement and analysis was continued on single-spot LSP samples during this reporting period by using two different methods: Vickers microhardness test and nanoindentation. Vickers microhardness test is a mature technique which could obtain the hardness at the micro level by simply comparing the load and the superficial area of the indentation. Figure 15 compares the 3D surface profiles of Al alloy surfaces after (a) the Vickers microhardness test and the (b) nanoindentation test. It can be observed that Vickers hardness affects a square area with a side length of 30 μm and a depth of 2.5 μm, while nanoindentation affects a triangle area with a side length of ~ 2 μm and a depth of 0.5 μm. Since the LSP-affected area and depth are nearly 1 mm diameter and 1 mm depth, respectively, both nanoindentation and the Vickers microhardness test can be used for localized hardness measurement.

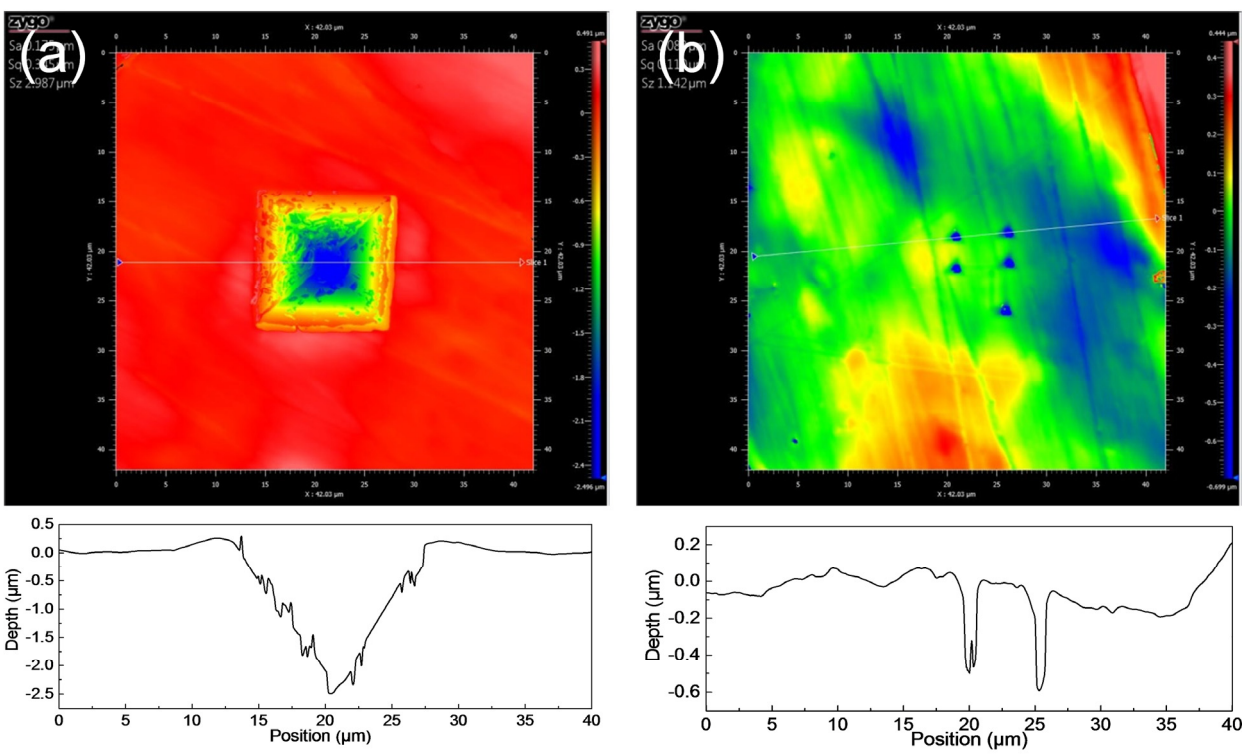

Fig. 15. 3D surface morphologies of Al alloy after (a) microhardness test and (b) nanoindentation test. Inserts in (a) and (b) show the cross-sectional height profiles along the lines in the corresponding images.

(A) Nano-indentation test

The nanoindentation measurement results for 304 stainless steel samples after LSP are presented in Fig. 16. Figure 16(a) shows the dependence of contact depth on LSP impact times. With the increase of LSP impacts, the contact depth decreases and tends to become stable. Figure 16b and 16c exhibit the dependence of the surface nanohardness and elastic modulus of the 304 SS samples on LSP impact time. Similar to the Al-Mg alloy and 310 SS (see the first quarterly report), the values of the surface nanohardness and elastic modulus for the laser-peened 304 SS are obviously larger than those of non-laser-peened samples. In addition, the values of surface nanohardness and elastic modulus of the sample increase with the increment of the LSP impact times. With a maximum of ten LSP impacts, the nanohardness and elastic modulus are increased by 18.4% and 313%, respectively, compared with that of the non-laser-peened region. The improved nanohardness and elastic modulus are considered to be favorable in enhancing the stiffness and the possible corrosion resistance of the stainless steel.

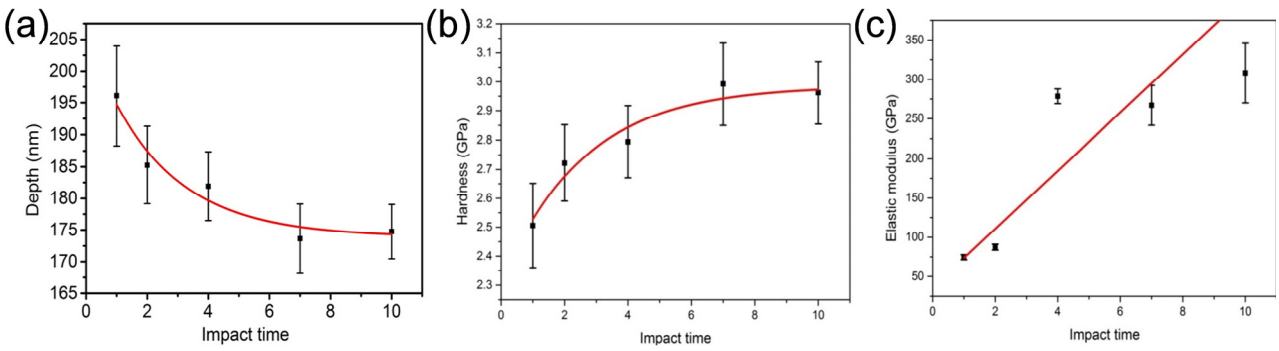

Fig. 16. The profiles of the (a) contact depth, (b) surface nanohardness, and (c) elastic modulus of the 304 SS samples as a function of LSP impact times.

(B) Microhardness test

The Vickers microhardness tests were carried out on three kinds of laser-peened materials, including Al-Mg alloy, 304 SS, and CS. As shown in Fig. 17a-c, to realize precise measurement of Vickers microhardness, the load curve dependence of hardness is first measured on non-laser-peened areas for (a) Al-Mg alloy, (b) 304 SS, and (c) CS. The standard is that the loads at the flat area of the curve where the hardness does not change with different loads are suggested for a normal test. For our conditions, a load of 0.05 kg was selected for all samples, where the hardness value was close to normal. The load could also enable easy multiple tests in the small test areas.

Figures 17(d-e) show the Vickers microhardness as a function of LSP impacts for (d) Al-Mg alloy, (e) 304 SS, and (f) CS, respectively. The values of the surface microhardness for the laser-peened Al-Mg alloy and 304SS samples were both obviously larger than those of samples without LSP. In addition, the surface microhardness of the sample increases with the increment

of the LSP impacts. With a maximum of five LSP impacts, the microharnesses of laser-peened Al-Mg alloy and 304 SS increased by 20.6% and 39.3%, respectively. The microhardness measurement results were similar to the nanoindentation measurement results, confirming that the surface hardness is improved by LSP and increased with the increment of the LSP impacts. For carbon steel, the Vickers microhardness does not obviously increase and even decreases with four LSP impacts, which may be attributed to the stiffness of carbon steel and need to be confirmed by further increasing LSP impact times.

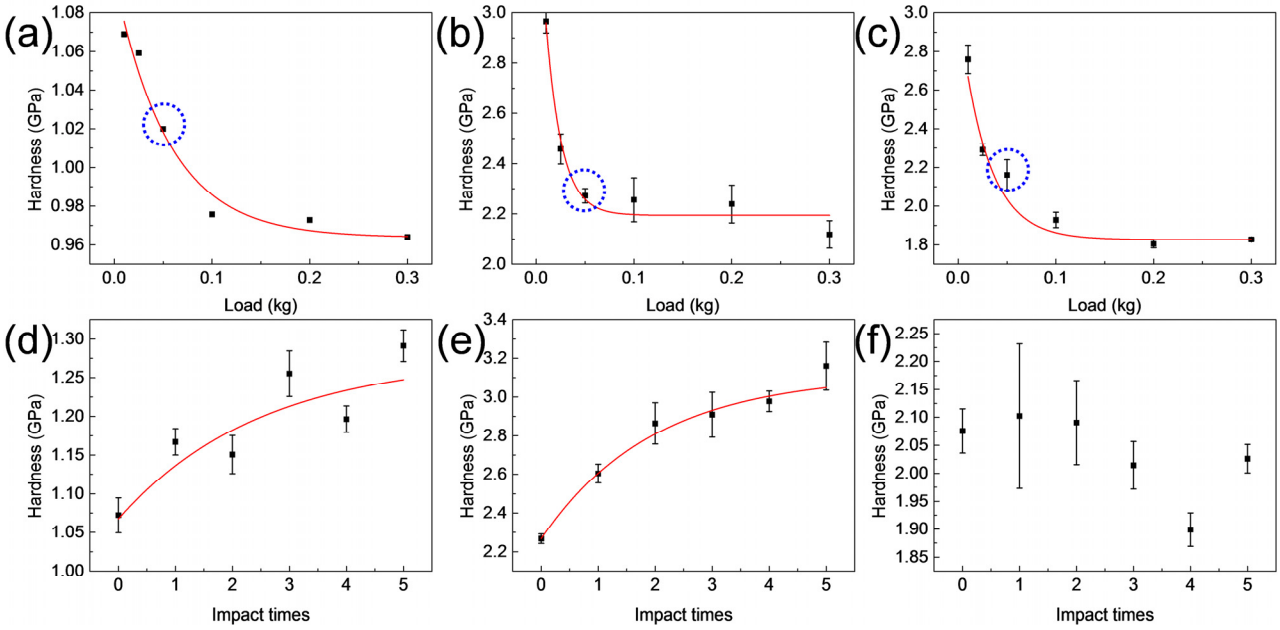

Fig. 17. (a-c) Load curves for (a) Al-Mg alloy, (b) 304 SS, and (c) CS. (d-f) Corresponding Vickers microhardness as a function of LSP impacts for (d) Al-Mg alloy, (e) 304 SS, and (f) CS.

2.2.4 Residual stresses induced by LSP

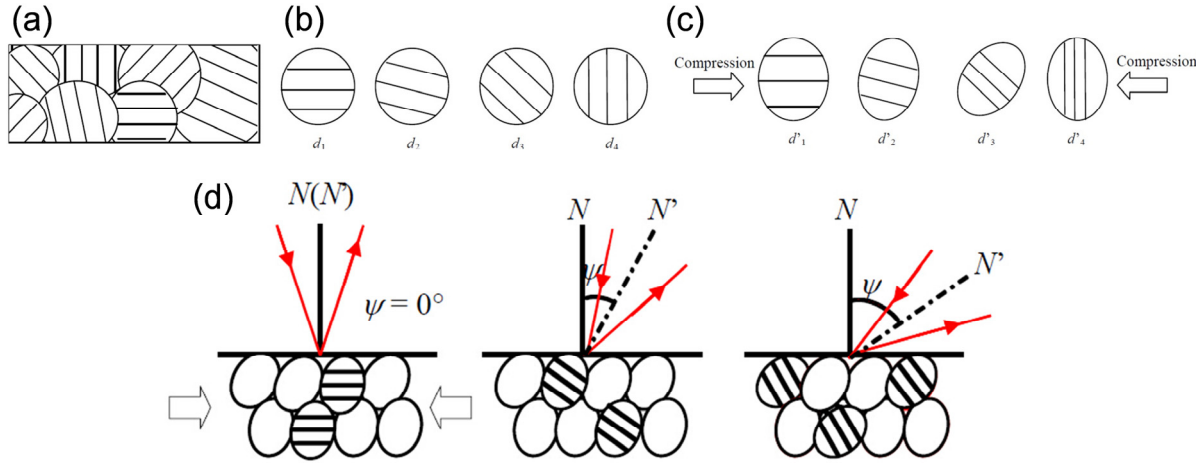

Fig. 18. Schematic of crystal oriented in (a) random directions in polycrystalline material, (b) different crystal orientation under stress-free conditions, (c) and after compressive stress with plastic deformation (c). (d) XRD theory model for residual stress measurement. [5]

Compressive residual stress is an important characterization for metal corrosion, since it could effectively prevent crack generation on the protective oxidization layer on metal surfaces and thus increase the corrosion resistance significantly, especially for stress corrosion cracking. The residual stresses after LSP processing were determined using a nondestructive technique, X-ray diffraction (XRD) $\sin^2\psi$ method. The principle of X-ray diffraction $\sin^2\psi$ method is shown in Fig. 18. As we know, metals are polycrystalline materials composed of numerous crystal particles oriented in random directions (Fig. 18a). Under stress free conditions (Fig. 18b), lattice spacing d1=d2=d3=d4; after compressive stress with plastic deformation (Fig. 18c), d1>d2>d3>d4. This lattice spacing change at different directions reflects the residual stress and could be measured by XRD through changing ψ (Fig. 18d).

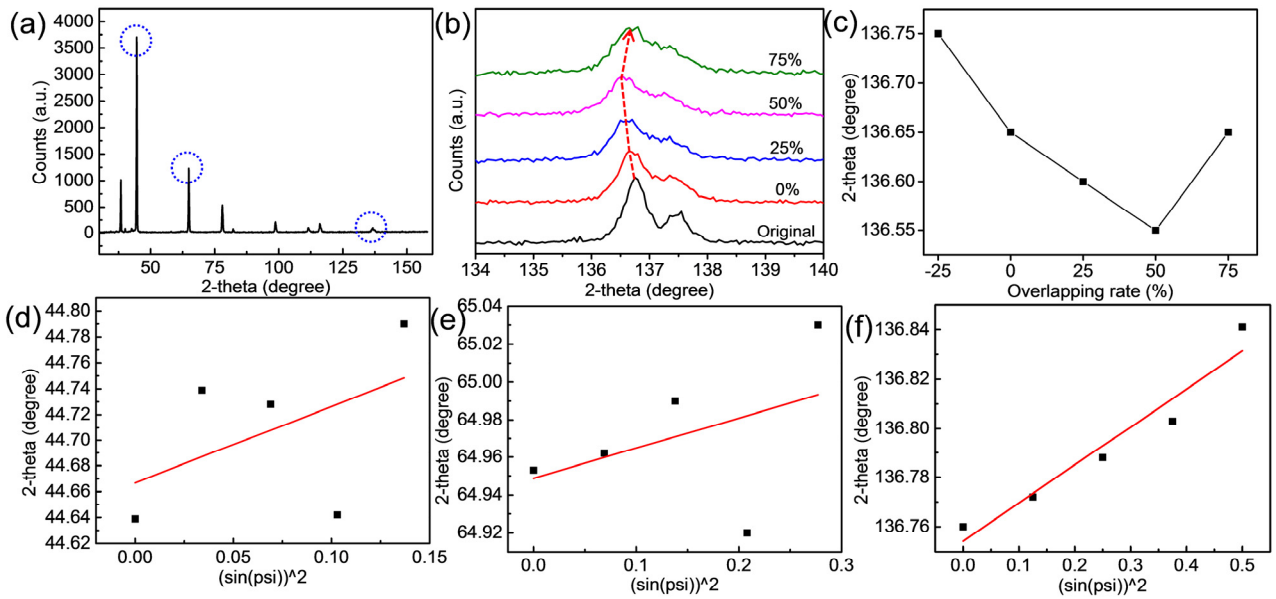

Fig. 19. (a) XRD pattern for Al alloy. (b, c) Diffraction peak position versus laser overlapping rate. 2-theta versus sin2ψ plot at different 2-theta of (b) 44.5°, (c) 64.9°, and (d) 136.7°.

Different metals have different peaks in XRD patterns due to their specific compositions and structures (Fig. 19(a)) with dashed blue circles to mark the 2-theta (2θ) angle of 44.5°, 64.9°, and 136.7° from left to right). Fig. 19(b) and 19(c) show the 2-theta shift (no offset) without LSP and with LSP of 0% to 75% overlapping rate, which might be induced by the different residual stresses. The selection of a peak for measurement is of great importance for the accuracy of the measured residual stress value. Figure 19(d-f) compare 2-theta versus sin2ψ plot at different 2-theta of (d) 44.5°, (e) 64.9°, and (f) 136.7°. The linear fitting results were 0.596 ± 0.608, 0.161 ± 0.197, and 0.154 ± 0.022, respectively, corresponding to residual stress values of -676 ± 883 MPa, -128 ± 176 MPa, and -27 ± 5 MPa, respectively. The error of calculation at 44.5° is the highest, and it decreases with the increase of 2-theta. At 136.7°, the error of calculation is about 18.5% and could be accepted. Therefore, a diffraction peak with 2-theta larger than 120° should be chosen for

the residual stress measurements by the 2-theta-$\sin^2\psi$ method.

Figure 20 shows the dependence of residual stress on the laser overlapping rate and LSP impact times for Al-Mg alloy. The residual stresses were measured by XRD with Cu as the anode target, and the selected peak (2θ) was 136.7°. The values of surface residual stress for the laser-peened samples were obviously larger than those for the non-laser-peened samples. With an increased overlapping rate from 0 to 50% during the large area LSP process, the surface residual stress obviously increased. However, when the overlapping rate reached 75%, there was a little reduction of the surface residual stress. The reason is that the 75% overlapping rate destroyed the sacrificial layer and induced ablation damage directly on the sample surface. In addition, no obvious change was observed for the surface residual stress by increasing impact time from one to two. The laser-peened samples with overlapping rates of 0 and 25%, the surface residual stresses were decreased by 42.2% and 38.2%, respectively; while the surface residual stresses for the laser-peened samples with overlapping rates of 50 and 75% were increased by 9.5% and 15.6%, respectively. Therefore, a 50% overlapping rate and one impact time can be selected for the large area LSP treatment of metal samples due to the LSP effect and the work efficiency.

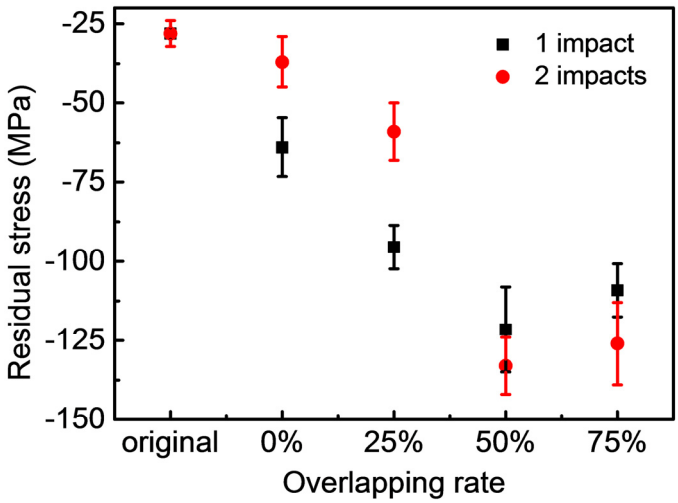

Fig. 20. The dependence of residual stresses on laser overlapping rates and LSP impact times.

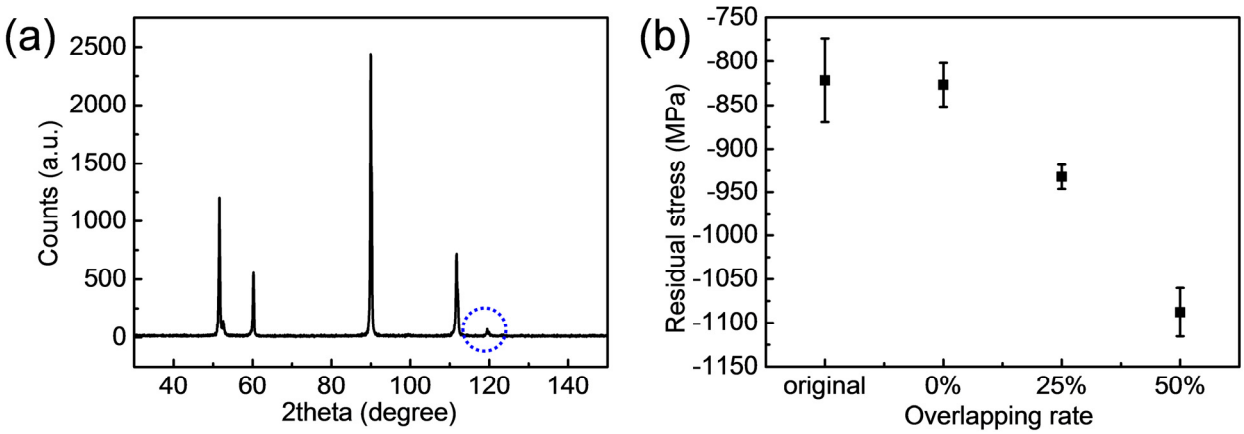

Fig. 21. (a) XRD pattern for 304 SS measured by Cr target. Dashed blue circle in (a) indicates the 2-theta angle for the residual stress measurement. (b) The dependence of residual stresses on laser overlapping rates.

The effect of the overlapping rate on the surface residual stress of the 304 SS surface was also investigated. The residual stresses were measured by XRD with Cr as the anode target. Figure 21(a) shows the XRD pattern of 304 SS. The diffraction peak at 2θ of 119.5^{o} marked with a dashed blue circle was selected for residual stress calculation. The values of surface residual stress for the laser-peened 304SS are larger than those for the non-laser-peened SS samples. With an increasing overlapping rate from 0 to 50% during the large area LSP process, the surface residual stress obviously increases. Compared to the original sample, the surface residual stresses of the laser-peened samples with overlapping rates of 0%, 25%, and 50%, are increased by 0.61%, 13.5%, and 32.4%, respectively. It is obvious that the main trends of residual stress distribution for 304 SS and Al-Mg alloy are the same. The 50% overlapping rate is also the best parameter to induce high residual stress on 304 SS material.

Key outcomes

In this reporting period, the experimental setup for LSP has been improved. The processing parameters (including laser energy, spot size, wavelength, and sacrificial coating) for LSP have been optimized. The effects of LSP on the surface topography, nano-/microhardness, elastic modulus, and surface residual stresses of the samples manufactured by Al-Mg alloy, stainless steel, and carbon steel have been experimentally investigated and analyzed. Some important conclusions have been summarized as follows:

(1) The experimental setup for the LSP system has been improved. First, the 3D stage used to hold the sample has been changed from a motor-controlled, six-axis work stage to a three-axis work stage with faster speed of movement and a larger moving range. Second, a new pump-based, water-cycle system has been implemented into the LSP system to form a thin water layer on the sample surface, which has the advantages of saving water and precisely controlling the water layer thickness.

(2) The effects of laser processing parameters (including laser energy, spot size, and wavelength) on LSP in metal components have been systemically investigated. It was found that the laser spot diameter can be varied and limited by the laser power available. The spot diameter is increased/decreased with the increment/decrement of laser power. According to the 3D profiler study, both the dent depth and dent diameter were increased with the increment of LSP power. In addition, compared with the shorter wavelength (532nm), longer wavelength (1064nm) is found to be slightly more efficient for the LSP effect, which was considered to result from a higher dielectric breakdown threshold.

(3) Metal surface morphology and microstructure can be effectively controlled by LSP. For example, micro-holes/protrusions with different sizes, shapes, and densities, can be selectively generated on the metal surface by LSP with modified black tape as the sacrificial layer. The result will help to avoid undesired micro-dents/protrusions defects forming on the

laser-peened metal surface. In addition, the laser-peen forming phenomenon has been observed during the large area LSP process. It is considered that the deep compressive stress achieved by LSP leads to the formation of tighter curvatures.

(4) For Al-Mg alloy and 304 SS, the values of surface nano-/microhardness for the laser-peened samples were obviously larger than those for the non-laser-peened samples. In addition, the values of surface nano-/microhardness were increased with the increment of LSP impact times. For carbon steel, the microhardness is nearly unchanged, which needs further research in the future. The improvement of the surface nano-/microhardness was considered to be favorable for improving the stiffness and corrosion resistance of these components used for pipeline construction.

(5) The effects of the overlapping rate and impact times on surface residual stress have been investigated on Al-Mg alloy and 304 SS. The values of surface residual stress for the laser-peened samples were obviously larger than those for the non-laser-peened samples. With increasing overlapping rate from 0 to 50% during the large area LSP process, the surface residual stress obviously increased both for Al-Mg alloy and 304 SS. However, when the overlapping rate reached 75%, there was a little reduction of the surface residual stress because of the destruction of the sacrificial layer and ablation damage on the sample surface. In addition, no obvious change was observed for the surface residual stress of the Al-Mg alloy by increasing the impact time from one to two. Therefore, a 50% overlapping rate and one impact time can be selected for a large area LSP treatment of metal samples due to the LSP effect and efficiency.

(b) Description of any Problems/Challenges

No problems were experienced during this reporting period.

(c) Planned Activities for the Next Quarter

The objectives and activities specifically planned to be accomplished during the next period (April 1, 2015, to June 30, 2015) are listed in Table 5.

Table 5. The planned objectives and activities for the second quarter

Objectives	Activities
(a) Corrosion resistance test of laser-peened samples	1) Sample preparation for the corrosion test. 2) Selection and preparation of corrosion solution. 3) Corrosion test and analysis of the laser-peened samples.
(b) Surface evaluation of laser-peened samples	1) To study the depth profile of the micro-/nanohardness distribution for the laser-peened sample using microhardness and nanoindenation technique. 2) To conduct the depth profile compressive residual stress measurement of the laser-peened sample using X-ray diffraction

	$\sin^2\Psi$ method. 3) To investigate the grain refinement mechanism of LSP impacts on stainless steel by means of cross-sectional optical microscopy and transmission electron microscopy observation.
(c) LSP mechanism study	1) Laser-induced breakdown spectroscopy (LIBS) technique will be used td to study LSP process by measuring plasma development and expansion. 2) LIBS will also be used to measure the temperature and density of the LSP-induced plasma. 3) Analysis of LIBS results to demonstrate the LSP processing mechanism.

References

[1] Fairand, B. P.; Clauer, A. H., Effect of water and paint coatings on the magnitude of laser-generated shocks. *Optics Communications* **1976,** *18* (4), 588-591.

[2] Fairand, B. P.; Wilcox, B. A.; Gallagher, W. J.; Williams, D. N., Laser shock - induced microstructural and mechanical property changes in 7075 aluminum. *Journal of Applied Physics* **1972,** *43* (9), 3893-3895.

[3] Caslaru, R.; Guo, Y.; Sealy, M.; Chen, S., Fabrication and characterization of micro dent array produced by laser shock peening on aluminum surfaces. *Trans. NAMRI/SME* **2009,** *37*, 159-166.

[4] Charless S. montross, Tao Wei, Lin Ye, Graham Clark, Yiu-Wing Mai, Laser shock processing and its effects on microstructure and properties of metal alloys: a review. *International Journal of Fatigue* **2012**, 24, 1021-1036.

[5] Rigaku Residual Stress Analysis Group, Residual stress measurement.